ACS APPLIED MATERIALS & INTERFACES

Research Article

www.acsami.org

Nickel Hydroxide-Modified Sulfur/Carbon Composite as a High-Performance Cathode Material for Lithium Sulfur Battery

Xiao-Qing Niu,[†] Xiu-Li Wang,*[,†] Dong Xie,[†] Dong-Huang Wang,[†] Yi-Di Zhang,[†] Yi Li,[†] Ting Yu,[‡] and Jiang-Ping Tu[†]

[†]State Key Laboratory of Silicon Materials, Key Laboratory of Advanced Materials and Applications for Batteries of Zhejiang Province, and School of Materials Science and Engineering, Zhejiang University, Hangzhou, Zhejiang 310027, China

[‡]Division of Physics and Applied Physics, School of Physical and Mathematical Science, Nanyang Technological University, Singapore 637371, Singapore

ABSTRACT: Tailored sulfur cathode is vital for the development of a high performance lithium−sulfur (Li−S) battery. A surface modification on the sulfur/carbon composite would be an efficient strategy to enhance the cycling stability. Herein, we report a nickel hydroxide-modified sulfur/conductive carbon black composite ($Ni(OH)_2$@S/CCB) as the cathode material for the Li−S battery through the thermal treatment and chemical precipitation method. In this composite, the sublimed sulfur is stored in the CCB, followed by a surface modification of $Ni(OH)_2$ nanoparticles with size of 1−2 nm. As a cathode for the Li−S battery, the as-prepared $Ni(OH)_2$@S/CCB electrode exhibits better cycle stability and higher rate discharge capacity, compared with the bare S/CCB electrode. The improved performance is largely due to the introduction of $Ni(OH)_2$ surface modification, which can effectively suppress the "shuttle effect" of polysulfides, resulting in enhanced cycling life and higher capacity.

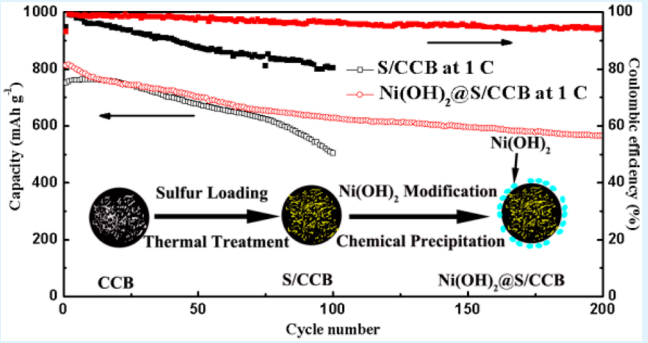

KEYWORDS: *lithium sulfur battery, nickel hydroxide, surface modification, cycle stability, sulfur cathode*

INTRODUCTION

Over the past decades, there has been rapid growth in developing green and sustainable energy sources because of the increasing environmental issues caused by fossil fuel and emerging consumer demand for portable electronics and electric vehicles (EVs).[1,2] Among various developed energy storage devices, rechargeable lithium-ion batteries (LIBs) are considered to be one of the most fascinating and widely used energy storage systems owing to their high capacity, high working voltage, long cycling life, and low toxicity.[3,4] However, most applications, especially the electric-transportation fields, require LIBs with both large energy density and high power density, which remains one of the most important challenges of modern electrochemistry. Unfortunately, the current cathode materials are incapable of this mission. For example, commercial transition metal oxide cathode materials, such as $LiFePO_4$,[5,6] $LiCoO_2$,[7] $LiMnO_2$,[8] and $LiNi_{1/3}Mn_{1/3}Co_{1/3}O_2$,[9,10] deliver specific capacities of lower than 220 mAh g^{-1} and energy densities of lower than 250 Wh kg^{-1}. Therefore, it is highly urgent to develop next-generation high-performance cathode materials with both high energy and power densities.

Recently, the lithium−sulfur (Li−S) battery has sparked great research interest, due to low cost, high theoretical specific capacity (1675 mAh g^{-1}), and large energy density (2500 Wh kg^{-1}), which are much higher than those of the commercial cathode materials.[11−14] Despite these merits, the further development of Li−S batteries is severely hindered by several obstacles: (1) the insulating nature of sulfur and polysulfides (Their poor electrical conductivity results in a low utilization of active sulfur and poor rate performance.);[15,16] (2) large volumetric expansion during the lithiation process, which could lead to cracking or fracturing of the electrodes as well as severe capacity fading during cycling;[16,17] (3) dissolution of polysulfides (Li_2S_n, $4 \leq n \leq 8$) resulting from the "shuttle effect".[18,19] It would cause loss of active materials and lower capacity, resulting in poor cyclic life, and low Coulombic efficiency.[20] Among these challenges, the "shuttle effect" is the main issue needed to be solved for fabricating advanced sulfur cathode materials.

To circumvent these drawbacks, construction of highly porous carbon supported sulfur (S/C) composite has been considered to be a promising strategy. These carbon materials including carbon black,[21] hierarchical porous carbon,[22−25] graphene,[26−28] or carbon nanotube/nanofiber[29−31] not only have been used as a host for accommodation of sulfur but also provide fast ion/electron transfer path. For example, He et al.[32] reported an ordered mesoporous carbon/sulfur electrode, with

Received: May 21, 2015
Accepted: July 9, 2015
Published: July 9, 2015

DOI: 10.1021/acsami.5b04408
ACS Appl. Mater. Interfaces 2015, 7, 16715−16722

an initial capacity of 995 and 550 mAh g^{-1} after 100 cycles at 1 C.

Albeit there are advantages of the S/C composite, the single combination of porous carbon materials and sulfur is still far from satisfactory due to the fact that the sulfur anchored in the carbon materials could also migrate outward and lose active materials over the extended cycling process. This will lead to obvious capacity fading during the cycling process. In recent years, chemical modifications on the surface of S/C composite electrode are demonstrated to be a useful approach in encapsulating nanostructured sulfur and suppressing the dissolution of polysulfides. Previously, Song et al.[33] employed a cetyltrimethylammonium bromide (CTAB)-modified sulfur−graphene oxide (S−GO) nanocomposite as the cathode material for the Li−S battery. The surface modification by CTAB was proven to effectively entrap polysulfides, resulting in a low capacity decay of 0.039% per cycle during the 1500 cycling process at 1 C. Gao and co-workers[34] and Chen and co-workers[35] adopted polyaniline as the modification layer on the surface of the sulfur/carbon composite, and improved electrochemical performances were obtained compared with the bare sulfur/carbon. Meanwhile, Nazar and co-workers[36] utilized polar manganese dioxide (MnO_2) to confine and adsorb the soluble polysulfides. A high initial capacity of 1300 mAh g^{-1} at 0.05 C and decay rate of 0.036% per cycle over 2000 cycles at 2 C were obtained. The above results demonstrate that surface engineering or modification is a useful way for suppressing the shuttle effect to enhance the electrochemical performances of sulfur cathode.

Inspired by the encouraging results above, herein, we report a novel modification work for the construction of advanced sulfur electrode, in which conductive carbon black (CCB) serves as the conductive scaffold for the active sulfur and $Ni(OH)_2$ nanoparticles act as the surface modifier. Compared with the bare S/CCB electrode, the $Ni(OH)_2$-modified S/CCB electrode ($Ni(OH)_2$@S/CCB) exhibits better capacity retention and higher Coulombic efficiency due to the effective suppression of the polysulfides shuttle.

EXPERIMENTAL SECTION

Preparation of the $Ni(OH)_2$@S/CCB Composite. Scheme 1 illustrates the fabrication process of the $Ni(OH)_2$-modified sulfur/conductive carbon black nanosphere ($Ni(OH)_2$@S/CCB). Two main procedures are required for the fabrication process. (1) The synthesis of S/CCB composite by thermal treatment. In a typical synthesis, the conductive carbon black and sublimed sulfur with the mass ratio of m_s/m_c = 3/2 were mixed by grinding in the mortar; then, the homogeneously mixed powders were sealed in an evacuated quartz tube and heated at 155 °C for 24 h under Ar, in order to allow the melted sulfur to diffuse into the pores of the CCB. The obtained S/CCB composites were then ground for the following treatment. (2) Uniform modification of the precursors with $Ni(OH)_2$ via a facial chemical precipitation method. Generally, 4 mmol of $NiSO_4 \cdot 6H_2O$ and 0.3 g of S/CCB composites were dissolved in 90 mL of deionized water (DIW) to form a stable solution; then, 10 mL of concentrated ammonia was added and kept stirring for 1 h at room temperature. After that, the product was sequentially washed with DIW and dried in a vacuum oven at 60 °C overnight.

Scheme 1. Schematic Illustration for the Formation of S/CCB and $Ni(OH)_2$@S/CCB Composite

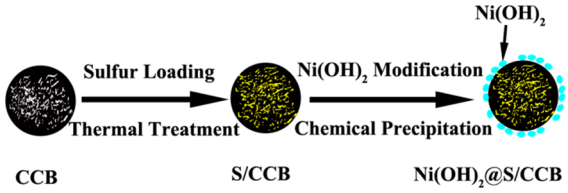

Material Characterization. X-ray diffraction (XRD) patterns of the materials were recorded in the 2θ range from 10° to 70° using RIGAKUD/Max−2550 with Cu Kα radiation. The Raman spectrum was scanned from 800 to 2200 cm^{-1} on an argon laser Raman spectroscopy using 514 nm laser wavelengths (Laber Raman Series, HR−800). X-ray photoelectron spectroscopy (XPS) tests were conducted on a ESCALAB 250Xi system; all peaks were referenced to the C 1s line at binding energy of 284.8 eV, and the core peaks were analyzed using a nonlinear Shirley-type background. The related peak positions and areas were optimized by a weighted least-squares fitting method. Thermal gravimetric analysis (TGA) was carried out on a Mettler ToledoSDTQ600 instrument employing a heating rate of 10 °C min^{-1} from room temperature to 500 °C under N_2 atmosphere to determine the sulfur content in the materials. Inductively coupled plasma atomic emission spectrometry (ICP−AES) was used to identify the amount of $Ni(OH)_2$ in the composite using the IRIS Intrepid II, Thermo Fisher Scientific. To characterize the structures and morphologies of the as-synthesized materials, scanning electron microscopy (SEM) studies were performed on a SU−70 field emission scanning electron microscopy instrument, while transmission electron microscopy (TEM) was carried out on a JEM 2100F High-resolution TEM (HRTEM).

Electrochemical Measurements. The electrode slurry was prepared by mixing $Ni(OH)_2$@S/CCB composites with conductive carbon black and polyvinylidene fluoride (PVDF) at the weight ratio of 8:1:1 in *N*-methyl-2-pyrrolidone (NMP). The electrode was prepared by coating the slurry onto an aluminum foil and dried at 60 °C for 24 h in vacuum to remove the absorbed water of the composite. The electrolyte was 1 M bis (trifluoromethane) sulfonamide lithium salt (LiTFSI) in a mixed solvent of 1,3-dioxolane (DOL) and 1,2-dimethoxyethane (DME) with a volume ratio of 1:1, including 1 wt % $LiNO_3$ as an electrolyte additive. Lithium metal was used as the counter and reference electrodes, and a polypropylene microporous film (Cellgard 2300) was used as the separator. 2025-type coin cells were assembled in a glovebox filled with Ar. The average S mass loading of the cathode is about 1.5 mg/cm^2. The discharge/charge performances were tested on a LAND battery program−control test system (Wuhan, China) in a potential range between 1.6 and 2.8 V at room temperature. Cyclic voltammetry (CV) measurements were performed with a CHI 660D electrochemical workstation in the potential range of 1.2−3.0 V (Li/Li^+) at a scan rate of 0.1 mV s^{-1}. Electrochemical impedance spectroscopy (EIS) measurements were conducted in the frequency ranges from 100 kHz to 10 mHz by applying an AC signal of 5 mV on a CHI 660D electrochemical workstation (Shanghai Chenhua instrument Co., LTD). The cathodes were overdischarged to 1.2 V in the first two cycles for activation, and the third cycle is considered as the first cycle of the cycle tests in this work. The specific capacity is calculated on the basis of the mass of sulfur in the electrode.

RESULTS AND DISCUSSION

The XRD patterns of the commercial CCB, sublimed sulfur (S), as-prepared $Ni(OH)_2$, S/CCB composite, and $Ni(OH)_2$@S/CCB composite are shown in Figure 1a. For the commercial CCB, the strong signal at 25° demonstrates that the CCB is partially graphitized and the weak signal at 42° suggests the quasi-amorphous frameworks.[37] The sharp diffraction peaks of sublimed sulfur denote that S exists in an *Fddd* orthorhombic structure.[25] For the $Ni(OH)_2$ synthesized by the chemical precipitation method, the weak and broad reflection peaks at 19.0°, 33.1°, 38.6°, and 59.2° can be indexed as (001), (100), (101), and (110) crystal planes of a hexagonal $Ni(OH)_2$ phase, respectively, which are in accordance with that of the standard

DOI: 10.1021/acsami.5b04408
ACS Appl. Mater. Interfaces 2015, 7, 16715−16722

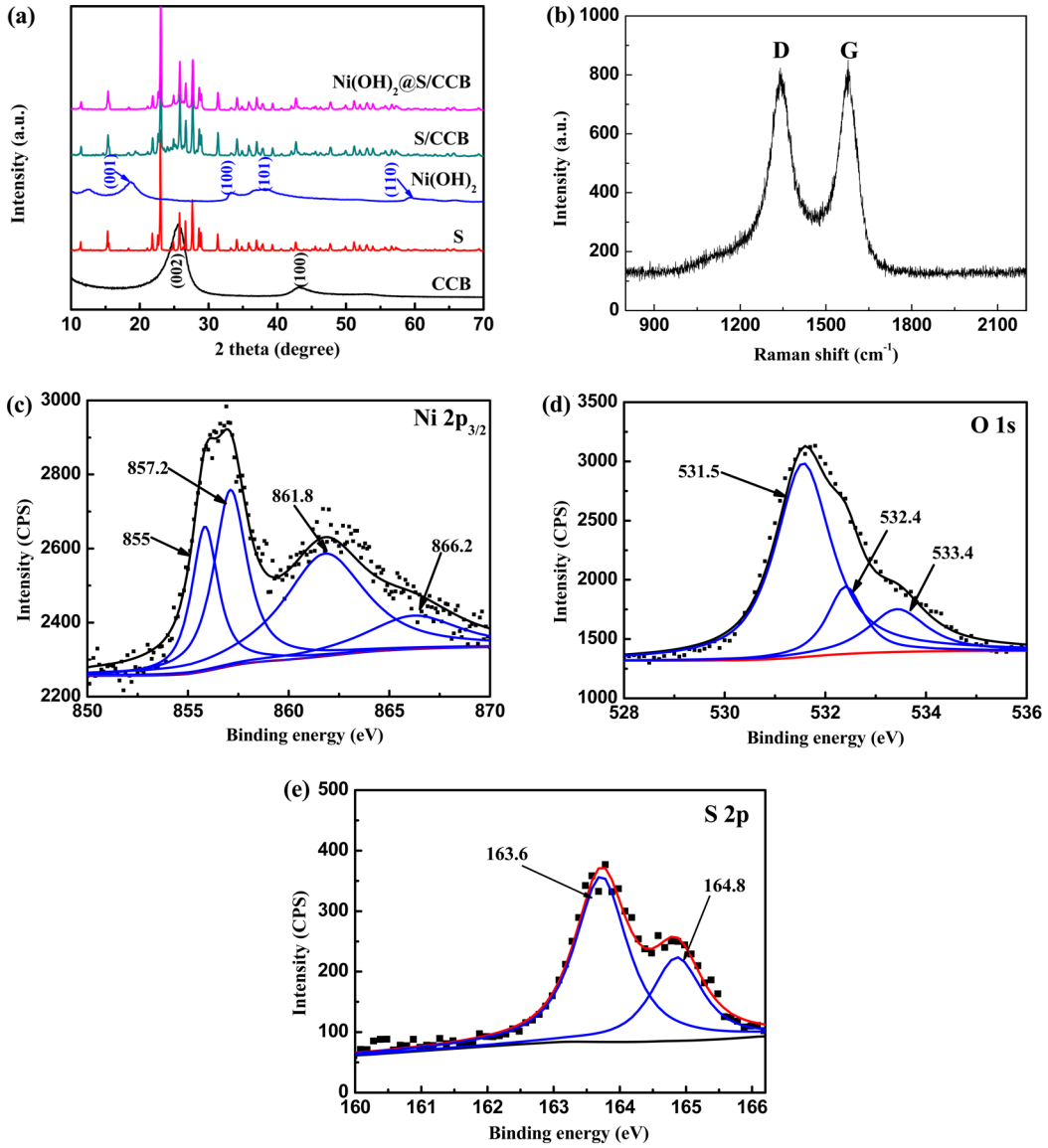

Figure 1. (a) XRD patterns of the pristine CCB, elemental sulfur, synthesized $Ni(OH)_2$, S/CCB composite, and $Ni(OH)_2$@S/CCB composite. (b) Raman spectrum of the $Ni(OH)_2$@S/CCB composite (800−2200 cm^{-1}). XPS high-resolution spectra of (c) Ni $2p_{3/2}$, (d) O 1s, and (e) S 2p obtained from $Ni(OH)_2$@S/CCB composite.

values (JCPDS 01−1047). The XRD patterns of S/CCB composite and $Ni(OH)_2$@S/CCB composite can be well indexed by the orthorhombic structure of S; neither CCB pattern nor $Ni(OH)_2$ pattern is observed. This is probably due to the weak peaks from CCB and $Ni(OH)_2$ being overlapped with those of S. XRD spectra confirm that S in the S/CCB composite and $Ni(OH)_2$@S/CCB composite is highly crystalline, and no new phase is generated during the two-step fabrication process. To further investigate the carbon matrix in the $Ni(OH)_2$@S/CCB composite, Raman spectroscopy was carried out, as shown in Figure 1b. The D peak at ~1341 cm^{-1} represents disordered carbon, and the G peak at ~1577 cm^{-1} corresponds to the graphitic carbon.[38] The intensity ratio of D peak and G peak indicates that the CCB is partially graphitized, consistent with the XRD results, and the partially graphitized carbon could facilitate the transport of electrons from/to the poorly conducting sulfur.[26] To confirm the existence of $Ni(OH)_2$ in the $Ni(OH)_2$@S/CCB composite, XPS tests were applied. Figure 1c,d shows the Ni $2p_{3/2}$ and O 1s XPS spectra of the $Ni(OH)_2$@S/CCB composite. The Ni $2p_{3/2}$ spectrum (Figure 1c) displays four main contributions at ~855.0, ~857.2, ~861.8, and ~866.2 eV, which are in accord with the Ni $2p_{3/2}$ in $Ni(OH)_2$. For the O 1s (Figure 1d), it shows a strong contribution at 531.5 eV, which can be attributed to the O from the hydroxide ions.[39,40] The low peaks in the O 1s spectrum are ascribed to carbonate ions contamination and hydroxyl on the surface of the composite.[41] All of the above results imply that $Ni(OH)_2$ is formed in the $Ni(OH)_2$@S/CCB composite. Additionally, the XPS spectrum of S 2p for $Ni(OH)_2$@S/CCB is measured (Figure 1e); the S 2p peak exhibits two peaks at 164.8 eV (S $2p_{1/2}$) and 163.6 eV (S $2p_{3/2}$), which matches with the typical peaks of the elemental sulfur.[42,43]

TGA was conducted to determine the sulfur content in the composites. As shown in Figure 2, sulfur begins to sublimate at its melting temperature and ends at about 330 °C. The as-synthesized $Ni(OH)_2$ is observed to exhibit three distinct weight loss profiles. The first one starts below 50 °C due to the

DOI: 10.1021/acsami.5b04408
ACS Appl. Mater. Interfaces 2015, 7, 16715−16722

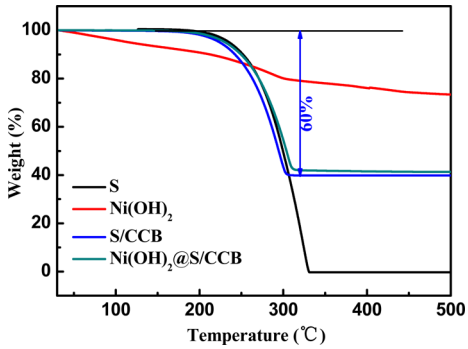

Figure 2. TGA curves of S, $Ni(OH)_2$, S/CCB composite, and $Ni(OH)_2$@S/CCB composite.

elimination of adsorbed water and intercalated water molecules, and the second major weight loss begins at 220 °C, which results from the decomposition of $Ni(OH)_2$ to NiO. A continued weight loss occurs at above 400 °C, which is probably attributed to the reduced decomposition of the NiO_2 formed at about 400 °C.[44] On the basis of the TGA curves, the content of S in the S/CCB composite is determined to be 60 wt %, which is consistent with the proportions of the added amount. The TG curve of the $Ni(OH)_2$@S/CCB composite is similar to that of the S/CCB composite with an approximate weight loss, owing to the low content of the $Ni(OH)_2$ in the $Ni(OH)_2$@S/CCB composite. In view of the fact that the weight loss range of $Ni(OH)_2$ is overlapped with sulfur, it is not possible to determine the sulfur content in the $Ni(OH)_2$@S/CCB composite only by TGA. Thus, ICP was used here to measure the Ni content in the Ni $(OH)_2$@S/CCB composite and the analysis shows 1.56 wt % of $Ni(OH)_2$ in the composite. Along with the fixed ratio of S and CCB (3/2), the final sulfur content in the $Ni(OH)_2$@S/CCB composite is 59.06 wt %.

Figure 3 presents the SEM and TEM images of the $Ni(OH)_2$ nanosheets, S/CCB composite, and $Ni(OH)_2$@S/CCB composite. The synthesized $Ni(OH)_2$ exhibits a sphere morphology constructed by numbers of densely packed and curved nanosheets (Figure 3a). The S/CCB composite appears as a particle aggregation of some small spheres with an average size of less than 100 nm (Figure 3b). It has been put forward that melted sulfur can diffuse into the pores of the CCB by a capillary force when heat-treated at 155 °C. After coating $Ni(OH)_2$ on the surface of the S/CCB composite (Figure 3c,d), the spherical morphology of the S/CCB could still remain. However, it is hard to identify the presence of the $Ni(OH)_2$ from the SEM images. To confirm the microstructure further, high-resolution TEM (HRTEM) images of the composites before and after the $Ni(OH)_2$ modification are shown in Figure 3e,f. The diameter of the CCB spheres with a partial graphite structure is about 50 nm. No crystalline sulfur is observed in the S/CCB composite; this is probably because sulfur is sublimated under the high energy electron beam.[27] In the $Ni(OH)_2$@S/CCB composite, the surface of the S/CCB nanophere is homogeneously anchored by many $Ni(OH)_2$ nanoparticles with a size of 1−2 nm, as shown in Figure 3f. To further confirm the structure and components in the $Ni(OH)_2$@S/CCB composite, elemental mappings of the nickel, carbon, sulfur, and oxygen of the $Ni(OH)_2$@S/CCB composite are conducted (Figure 3g). Carbon and sulfur are distributed uniformly in the composite; Ni and O are also detected in the surface of the composite, suggesting that sulfur

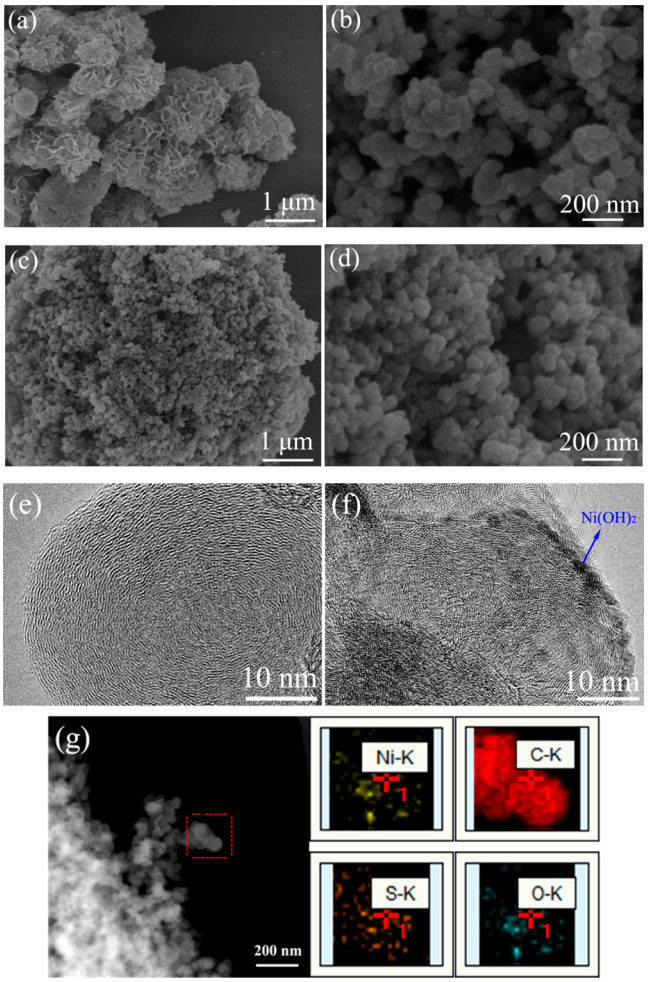

Figure 3. SEM images of (a) $Ni(OH)_2$; (b) S/CCB composite; (c, d) $Ni(OH)_2$@S/CCB composite. HRTEM images of (e) S/CCB composite and (f) $Ni(OH)_2$@S/CCB composite. (g) STEM and the mapping images of the $Ni(OH)_2$@S/CCB composite.

is well dispersed in the CCB pores, and $Ni(OH)_2$ is on the surface of the S/CCB composite, in agreement with the TEM result (Figure 3f). It is reported that chemical modification of the S/C surface by transition metal ions may change the nature of fundamental interactions between the host framework and polysulfides during the electrochemical process.[45] After being anchored with $Ni(OH)_2$, the composite has a stronger affinity for polysulfide ions, resulting in an effective retardation of polysulfides diffusion. As expected, the $Ni(OH)_2$ modified S/CCB composite will display better cycling performance and rate capacity.

The CV curves of S/CCB and $Ni(OH)_2$@S/CCB electrodes are displayed in Figure 4a,b. Two reduction peaks at potentials of ~2.28 and ~2.0 V (vs Li/Li^+) can be clearly observed for the S/CCB electrode. According to the electrochemical reaction mechanism of the elemental sulfur, the peak at around 2.28 V corresponds to the reduction of S to the soluble long-chain Li_2S_n ($4 \le n < 8$) and the peak at about 2.0 V is attributed to the conversion of long-chain polysulfides to the insoluble Li_2S_2/Li_2S. In its reverse process, one sharp oxidation peak at around 2.5 V can be observed, which can be assigned to the transformation of Li_2S_2/Li_2S to S.[46−48] To further study the electrochemical reaction mechanism, the third CV curves of the two electrodes are displayed in Figure 4b. Compared with the

DOI: 10.1021/acsami.5b04408
ACS Appl. Mater. Interfaces 2015, 7, 16715−16722

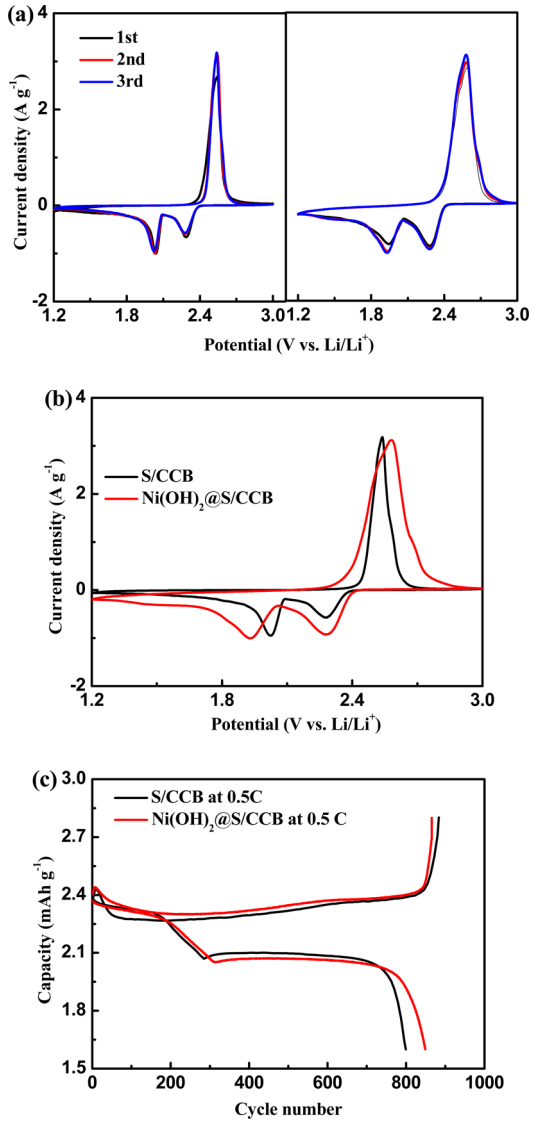

Figure 4. (a) The CV curves of S/CCB and $Ni(OH)_2$@S/CCB electrodes. (b) The third cycle of the CV curve for S/CCB electrode in comparison with $Ni(OH)_2$@S/CCB electrode. (c) The initial discharge/charge profiles of S/CCB and $Ni(OH)_2$@S/CCB electrodes at 0.5 C.

S/CCB electrode, the oxidation peak of the $Ni(OH)_2$@S/CCB electrode is positively shifted to ~2.58 V, while the conversion reaction of long-chain polysulfides to insoluble Li_2S_2/Li_2S starts from 1.93 V and continues to 1.2 V. This may be ascribed to the changed surface chemical environment of the S/CCB composite after $Ni(OH)_2$ modification, and the changed chemical environmental probably favors the interaction with the polysulfide anions.[49] The initial charge/discharge voltage profiles of the S/CCB electrode and $Ni(OH)_2$@S/CCB electrode at 0.5 C are shown in Figure 4c. Both electrodes display two typical discharge plateaus and one charge plateau of the sulfur electrode, which are consistent with the results of CV measurements. Besides, the Coulombic efficiency of the $Ni(OH)_2$@S/CCB electrode is 98.1%, which is much higher than that of the S/CCB electrode (90.5%).

An excellent cycling performance is a demonstration of effectively restraining the polysulfides shuttle reaction. As shown in Figure 5a, the initial discharge capacity is 897 mAh

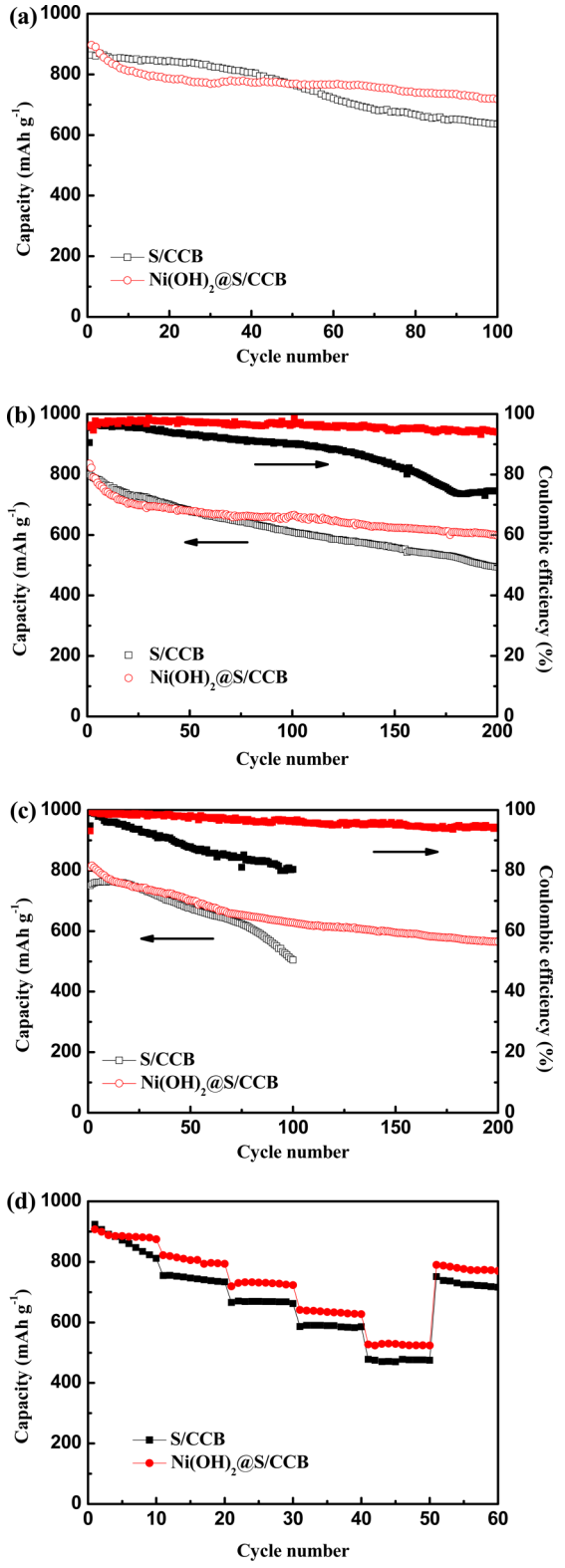

Figure 5. Cycling performances and Coulombic efficiencies of S/CCB and $Ni(OH)_2$@S/CCB electrodes at (a) 0.2 C; (b) 0.5 C, and (c) 1 C. (d) Rate capabilities of S/CCB and $Ni(OH)_2$@S/CCB electrodes.

g^{-1} for the $Ni(OH)_2$@S/CCB electrode at 0.2 C, which is 8% higher than that of the counterpart S/CCB electrode (834 mAh g^{-1}). In the S/CCB electrode, the discharge capacity stabilizes around 850 mAh g^{-1} between the 5th and 20th cycles, and the capacity decay rate is as slow as 0.07% per cycle during these

DOI: 10.1021/acsami.5b04408
ACS Appl. Mater. Interfaces 2015, 7, 16715−16722

cycles. However, the capacity decay rate increases to 0.31% per cycle in the following 80 cycles. This illustrates that the polysulfides can be trapped in the pores of CCB to some extent. However, without capping layer, polysulfide species can still migrate out during an extended cycling process.[48] On the contrary, the $Ni(OH)_2$@S/CCB electrode shows slightly faster decay at the very beginning, but the discharge capacity stabilizes after 20 cycles. The discharge capacity at the 20th cycle reaches 787 mAh g^{-1} for $Ni(OH)_2$-modified electrode. After that, a decay rate of only 0.11% per cycle is observed in the following 80 cycles and the capacity remains 718 mAh g^{-1} after 100 cycles. This suggests that polysulfides are better entrapped inside the carbon matrix due to the $Ni(OH)_2$ modification on the surface of the S/CCB composite. A similar phenomenon can be observed when the discharge current rate reaches 0.5 C (Figure 5b). The $Ni(OH)_2$-modified electrode shows a superior cycling performance in the long run, especially between the 100th and 200th cycles. The bare S/CCB electrode exhibits a capacity decay of 19% per 100 cycles, while the $Ni(OH)_2$-modified electrode decays 10% per 100 cycles. This further proves that the capacity decay accelerates in bare electrodes but slows down in those with $Ni(OH)_2$ modification. The possible reason for the remaining decay of 0.1% per cycle is that a fraction of the particles were not completely anchored with the $Ni(OH)_2$ so that a leakage path for the dissolution of polysulfides still exists.[48] Figure 5c shows the cycling performances of the electrodes at 1 C; the $Ni(OH)_2$@S/CCB electrode exhibits a favorable cycle stability with a capacity retention of 69.6% after 200 cycles, whereas the S/CCB electrode shows faster capacity decay. The better entrapment capability of the $Ni(OH)_2$ modification is also reflected in the improved Coulombic efficiency (Figure 5b,c). In the $Ni(OH)_2$@S/CCB electrode, the Coulombic efficiencies are above 94% after 200 cycles at both 0.5 and 1 C, much higher than that of the S/CCB electrode (75% after 200 cycles at 0.5 C and 80% after 100 cycles at 1 C). Furthermore, the rate capability of the S/CCB electrode and $Ni(OH)_2$@S/CCB electrode is also investigated. As shown in Figure 5d, the discharge capacities gradually decrease as the rate increased from 0.1 to 2 C for both of the electrodes. An improved rate performance for the $Ni(OH)_2$@S/CCB electrode is clearly observed; the discharge capacities of the $Ni(OH)_2$-modified electrode are stabilized at around 880, 800, 725, 630, and 520 mAh g^{-1} when tested at 0.1, 0.2, 0.5, 1, and 2 C, respectively. Particularly, when the current rate is switched abruptly from 2 to 0.1 C, the original capacity is largely recovered, illustrating the excellent rate performance of $Ni(OH)_2$@S/CCB electrode.[50]

To demonstrate the effectiveness of this unique configuration structure in improving the performance of the Li−S battery, electrochemical impedance spectroscopy (EIS) of the S/CCB and $Ni(OH)_2$@S/CCB electrodes after 20 cycles at 1 C is measured and shown in Figure 6. The Nyquist plots for both of the electrodes consist of two semicircles in the high−medium frequency region and a sloped line in the low frequency region, which are related to the impedance of passivation film, charge transfer resistance, and semi-infinite Warburg diffusion process, respectively.[38,51,52] It can be obviously observed from the figure that both the passivation film impedance and charge transfer resistance of the $Ni(OH)_2$@S/CCB electrode are much smaller than that of the S/CCB electrode, demonstrating more effective entrapment of dissolved sulfur and polysulfides as well as better charge transport and electrolyte infiltration, thereby mitigating the formation of the passivation layer (Li_2S_2/Li_2S) on the lithium anodes. Besides, the electrolyte resistance (the intercept at the real axis Z') of the $Ni(OH)_2$@S/CCB electrode is much smaller than the S/CCB electrode, indicating a better polysulfides-entrapment capability. The improved polysulfides-entrapment capacity verifies that this $Ni(OH)_2$@S/CCB electrode configuration is more promising to solve the persistent problem of capacity fade.

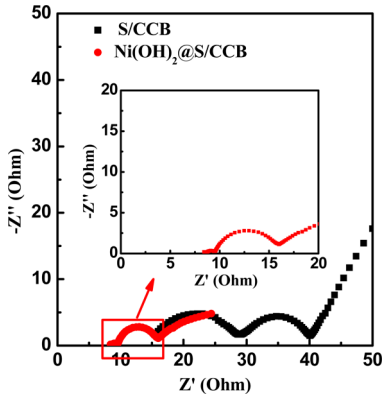

Figure 6. Nyquist plots of S/CCB and $Ni(OH)_2$@S/CCB electrodes after 20 cycles at 1 C (frequency range: 100 kHz to10 mHz).

CONCLUSIONS

In summary, we have demonstrated that the metal hydroxide modification at the S/C composite cathode is an effective approach for enhancement of sulfur cathode. In our case, the $Ni(OH)_2$ nanoparticles with size of 1−2 nm are strongly anchored on the surface of the S/CCB composite. Such a unique core/shell structure not only enhances electrical conductivity to facilitate charge transfer but also provides physical/chemical surface adsorption to inhibit polysulfides diffusion into the electrolyte. As a result, $Ni(OH)_2$@S/CCB has been demonstrated to show enhanced electrochemical behavior in terms of higher capacity and better cycling performance as compared to the S/CCB electrode. This nickel hydroxide shell modification work may pave the way for fabricating a high-performance sulfur cathode.

AUTHOR INFORMATION

Corresponding Author

*E-mail: wangxl@zju.edu.cn.

Notes

The authors declare no competing financial interest.

ACKNOWLEDGMENTS

This work is supported by National Natural Science Foundation of China (No. 51271167) and Program for Innovative Research Team in University of Ministry of Education of China (No. IRT13037). T.Y. is thankful for the support from A*Star SERC PSF grant 1321202101 and MOE Tier 2 MOE2012-T2-2-049.

REFERENCES

(1) Aricò, A. S.; Bruce, P.; Scrosati, B.; Tarascon, J. M.; Van Schalkwijk, W. Nanostructured Mmaterials for Advanced Energy Conversion and Storage Devices. *Nat. Mater.* **2005**, *4*, 366−377.

(2) Winter, M.; Brodd, R. J. What Are Batteries, Fuel Cells, and Supercapacitors? *Chem. Rev.* **2004**, *104*, 4245−4270.

DOI: 10.1021/acsami.5b04408
ACS Appl. Mater. Interfaces 2015, 7, 16715−16722

(3) Marom, R.; Amalraj, S. F.; Leifer, N.; Jacob, D.; Aurbach, D. A Review of Advanced and Practical Lithium Battery Materials. *J. Mater. Chem.* **2011**, *21*, 9938−9954.
(4) Tarascon, J. M.; Armand, M. Issues and Challenges Facing Rechargeable Lithium Batteries. *Nature* **2001**, *414*, 359−367.
(5) Liu, W. L.; Tu, J. P.; Qiao, Y. Q.; Zhou, J. P.; Shi, S. J.; Wang, X. L.; Gu, C. D. Optimized Performances of Core−Shell Structured $LiFePO_4$/C Nanocomposite. *J. Power Sources* **2011**, *196*, 7728−7735.
(6) Fedorková, A.; Oriňáková, R.; Oriňák, A.; Wiemhöfer, H. D.; Kaniansky, D.; Winter, M. Surface Treatment of $LiFePO_4$ Cathode Material with PPy/PEG Conductive Layer. *J. Solid State Electrochem.* **2010**, *14*, 2173−2178.
(7) Cao, Q.; Zhang, H. P.; Wang, G. J.; Xia, Q.; Wu, Y. P.; Wu, H. Q. A Novel Carbon−Coated $LiCoO_2$ as Cathode Material for Lithium Ion Battery. *Electrochem. Commun.* **2007**, *9*, 1228−1232.
(8) Koetschau, I.; Richard, M.; Dahn, J.; Soupart, J.; Rousche, J. Orthorhombic $LiMnO_2$ as A High Capacity Cathode for Li−Ion Cells. *J. Electrochem. Soc.* **1995**, *142*, 2906−2910.
(9) Ohzuku, T.; Makimura, Y. Layered Lithium Insertion Material of $LiCo_{1/3}Ni_{1/3}Mn_{1/3}O_2$ for Lithium−Ion Batteries. *Chem. Lett.* **2001**, *30*, 642−643.
(10) Shi, S. J.; Tu, J. P.; Mai, Y. J.; Zhang, Y. Q.; Gu, C. D.; Wang, X. L. Effect of Carbon Coating on Electrochemical Performance of $Li_{1.048}Mn_{0.381}Ni_{0.286}Co_{0.286}O_2$ Cathode Material for Lithium−Ion Batteries. *Electrochim. Acta* **2012**, *63*, 112−117.
(11) Barchasz, C.; Leprêtre, J. C.; Alloin, F.; Patoux, S. New Insights into the Limiting Parameters of the Li/S Rechargeable Cell. *J. Power Sources* **2012**, *199*, 322−330.
(12) Barchasz, C.; Mesguich, F.; Dijon, J.; Leprêtre, J. C.; Patoux, S.; Alloin, F. Novel Positive Electrode Architecture for Rechargeable Lithium/Sulfur Batteries. *J. Power Sources* **2012**, *211*, 19−26.
(13) Liang, X.; Wen, Z. Y.; Liu, Y.; Wang, X. Y.; Zhang, H.; Wu, M. F.; Huang, L. Z. Preparation and Characterization of Sulfur−Polypyrrole Composites with Controlled Morphology as High Capacity Cathode for Lithium Batteries. *Solid State Ionics* **2011**, *192*, 347−350.
(14) Wang, J. Z.; Lu, L.; Choucair, M.; Stride, J. A.; Xu, X.; Liu, H. K. Sulfur−Graphene Composite for Rechargeable Lithium Batteries. *J. Power Sources* **2011**, *196*, 7030−7034.
(15) Bresser, D.; Passerini, S.; Scrosati, B. Recent Progress and Remaining Challenges in Sulfur−Based Lithium Secondary Batteries−A Review. *Chem. Commun.* **2013**, *49*, 10545−10562.
(16) Evers, S.; Nazar, L. F. New Approaches for High Energy Density Lithium−Sulfur Battery Cathodes. *Acc. Chem. Res.* **2013**, *46*, 1135−1143.
(17) Yin, Y. X.; Xin, S.; Guo, Y. G.; Wan, L. J. Lithium−Sulfur Batteries: Electrochemistry, Materials, and Prospects. *Angew. Chem., Int. Ed.* **2013**, *52*, 13186−13200.
(18) Wang, D. W.; Zeng, Q. C.; Zhou, G. M.; Yin, L. C.; Li, F.; Cheng, H. M.; Gentle, I. R.; Lu, G. Q. M. Carbon−Sulfur Composites for Li−S Batteries: Status and Prospects. *J. Mater. Chem. A* **2013**, *1*, 9382−9394.
(19) Yang, Y.; Zheng, G. Y.; Cui, Y. Nanostructured Sulfur Cathodes. *Chem. Soc. Rev.* **2013**, *42*, 3018−3032.
(20) Kolosnitsyn, V.; Karaseva, E. Lithium−Sulfur Batteries: Problems and Solutions. *Russ. J. Electrochem.* **2008**, *44*, 506−509.
(21) Jeong, B. O.; Kwon, S. W.; Kim, T. J.; Lee, E. H.; Jeong, S. H.; Jung, Y. Effect of Carbon Black Materials on the Electrochemical Properties of Sulfur−Based Composite Cathode for Lithium−Sulfur Cells. *J. Nanosci. Nanotechnol.* **2013**, *13*, 7870−7874.
(22) Jung, D. S.; Hwang, T. H.; Lee, J. H.; Koo, H. Y.; Shakoor, R. A.; Kahraman, R.; Jo, Y. N.; Park, M. S.; Choi, J. W. Hierarchical Porous Carbon by Ultrasonic Spray Pyrolysis Yields Stable Cycling in Lithium−Sulfur Battery. *Nano Lett.* **2014**, *14*, 4418−4425.
(23) Choi, H. S.; Oh, J. Y.; Park, C. R. One Step Synthesis of Sulfur−Carbon Nanosheet Hybrids Via A Solid Solvothermal Reaction for Lithium Sulfur Batteries. *RSC Adv.* **2014**, *4*, 3684−3690.
(24) Li, X. L.; Cao, Y. L.; Qi, W.; Saraf, L. V.; Xiao, J.; Nie, Z.; Mietek, J.; Zhang, J. G.; Schwenzer, B.; Liu, J. Optimization of Mesoporous Carbon Structures for Lithium−Sulfur Battery Applications. *J. Mater. Chem.* **2011**, *21*, 16603−16610.
(25) Zhao, C. Y.; Liu, L. J.; Zhao, H. L.; Krall, A.; Wen, Z. H.; Chen, J. H.; Hurley, P.; Jiang, J. W.; Li, Y. Sulfur−Infiltrated Porous Carbon Microspheres with Controllable Multi−Modal Pore Size Distribution for High Energy Lithium−Sulfur Batteries. *Nanoscale* **2014**, *6*, 882−888.
(26) Chen, R. J.; Zhao, T.; Lu, J.; Wu, F.; Li, L.; Chen, J. Z.; Tan, G. Q.; Ye, Y. S.; Amine, K. Graphene−Based Three−Dimensional Hierarchical Sandwich−Type Architecture for High−Performance Li/S Batteries. *Nano Lett.* **2013**, *13*, 4642−4649.
(27) Liu, Y.; Guo, J. X.; Zhang, J.; Su, Q. M.; Du, G. H. Graphene−Wrapped Sulfur Nanospheres with Ultra−High Sulfur Loading for High Energy Density Lithium−Sulfur Batteries. *Appl. Surf. Sci.* **2015**, *324*, 399−404.
(28) Wang, Y. X.; Huang, L. C.; Sun, L. C.; Xie, S. Y.; Xu, G. L.; Chen, S. R.; Xu, Y. F.; Li, J. T.; Chou, S. L.; Dou, S. X. Facile Synthesis of a Interleaved Expanded Graphite−Embedded Sulphur Nanocomposite as Cathode of Li−S Batteries with Excellent Lithium Storage Performance. *J. Mater. Chem.* **2012**, *22*, 4744−4750.
(29) Chung, S. H.; Manthiram, A. High−Performance Li−S Batteries with an Ultra−Lightweight MWCNT-Coated Separator. *J. Phys. Chem. Lett.* **2014**, *5*, 1978−1983.
(30) Li, Q.; Zhang, Z. A.; Guo, Z. P.; Lai, Y. Q.; Zhang, K.; Li, J. Improved Cyclability of Lithium−Sulfur Battery Cathode Using Encapsulated Sulfur in Hollow Carbon Nanofiber@Nitrogen−Doped Porous Carbon Core−Shell Composite. *Carbon* **2014**, *78*, 1−9.
(31) Moon, S.; Jung, Y. H.; Jung, W. K.; Jung, D. S.; Choi, J. W.; Kim, D. K. Encapsulated Monoclinic Sulfur for Stable Cycling of Li−S Rechargeable Batteries. *Adv. Mater.* **2013**, *25*, 6547−6553.
(32) He, G.; Ji, X. L.; Nazar, L. F. High "C" rate Li−S Cathodes: Sulfur Imbibed Bimodal Porous Carbons. *Energy Environ. Sci.* **2011**, *4*, 2878−2883.
(33) Song, M. K.; Zhang, Y. G.; Cairns, E. J. A Long−Life, High−Rate Lithium/Sulfur Cell: A Multifaceted Approach to Enhancing Cell Performance. *Nano Lett.* **2013**, *13*, 5891−5899.
(34) Li, G. C.; Li, G. R.; Ye, S. H.; Gao, X. P. A Polyaniline−Coated Sulfur/Carbon Composite with an Enhanced High−Rate Capability as a Cathode Material for Lithium/Sulfur Batteries. *Adv. Energy Mater.* **2012**, *2*, 1238−1245.
(35) Wu, F.; Chen, J. Z.; Li, L.; Zhao, T.; Chen, R. J. Improvement of Rate And Cycle Performence by Rapid Polyaniline Coating of A MWCNT/Sulfur Cathode. *J. Phys. Chem. C* **2011**, *115*, 24411−24417.
(36) Liang, X.; Hart, C.; Pang, Q.; Garsuch, A.; Weiss, T.; Nazar, L. F. A Highly Efficient Polysulfide Mediator for Lithium−Sulfur Batteries. *Nat. Commun.* **2015**, *6*, 5682−5689.
(37) Zhang, K.; Zhao, Q.; Tao, Z. L.; Chen, J. Composite of Sulfur Impregnated in Porous Hollow Carbon Spheres as the Cathode of Li−S Batteries with High Performance. *Nano Res.* **2013**, *6*, 38−46.
(38) Zheng, S. Y.; Wen, Y.; Zhu, Y. J.; Han, Z.; Wang, J.; Yang, J. H.; Wang, C. S. In Situ Sulfur Reduction and Intercalation of Graphite Oxides for Li−S Battery Cathodes. *Adv. Energy Mater.* **2014**, *4*, 482−491.
(39) Grosvenor, A. P.; Biesinger, M. C.; Smart, R. S. C.; McIntyre, N. S. New Interpretations of XPS Spectra of Nickel Metal and Oxides. *Surf. Sci.* **2006**, *600*, 1771−1779.
(40) Biesinger, M. C.; Payne, B. P.; Lau, L. W.; Gerson, A.; Smart, R. S. C. X−ray Photoelectron Spectroscopic Chemical State Quantification of Mixed Nickel Metal, Oxide and Hydroxide Systems. *Surf. Interface Anal.* **2009**, *41*, 324−332.
(41) Stoch, J.; Gablankowska Kukucz, J. The Effect of Carbonate Contaminations on the XPS O 1s Band Structure in Metal Oxides. *Surf. Interface Anal.* **1991**, *17*, 165−167.
(42) Fu, Y. Z.; Manthiram, A. Core-shell Structured Sulfur-Polypyrrole Composite Cathodes For Lithium-Sulfur Batteries. *RSC Adv.* **2012**, *2*, 5927−5929.
(43) Choi, H. S.; Oh, J. Y.; Park, C. R. One Step Synthesis of Sulfur−Carbon Nanosheet Hybrids Via A Solid Solvothermal Reaction for Lithium Sulfur Batteries. *RSC Adv.* **2014**, *4*, 3684−3690.

DOI: 10.1021/acsami.5b04408
ACS Appl. Mater. Interfaces 2015, 7, 16715−16722

(44) Song, Q. S.; Tang, Z. Y.; Guo, H. T.; Chan, S. L. I. Structural Characteristics of Nickel Hydroxide Synthesized by a Chemical Precipitation Route under Different pH Values. *J. Power Sources* **2002**, *112*, 428−434.
(45) Zheng, J. M.; Tian, J.; Wu, D. X.; Gu, M.; Xu, W.; Wang, C. M.; Gao, F.; Engelhard, M. H.; Zhang, J. G.; Liu, J.; Xiao, J. Lewis Acid−Based Interactions between Polysulfides and Metal Organic Framework in Lithium Sulfur Batteries. *Nano Lett.* **2014**, *14*, 2345−2352.
(46) Zhou, W. D.; Yu, Y. C.; Chen, H.; DiSalvo, F. J.; Abruña, H. c. D. Yolk−Shell Structure of Polyaniline−Coated Sulfur for Lithium−Sulfur Batteries. *J. Am. Chem. Soc.* **2013**, *135*, 16736−16743.
(47) Xiao, L. F.; Cao, Y. L.; Xiao, J.; Schwenzer, B.; Engelhard, M. H.; Saraf, L. V.; Nie, Z.; Exarhos, G. J.; Liu, J. A Soft Approach to Encapsulate Sulfur: Polyaniline Nanotubes for Lithium−Sulfur Batteries with Long Cycle Life. *Adv. Mater.* **2012**, *24*, 1176−1181.
(48) Yang, Y.; Yu, G. H.; Cha, J. J.; Wu, H.; Vosgueritchian, M.; Yao, Y.; Bao, Z. N.; Cui, Y. Improving the Performance of Lithium−Sulfur Batteries by Conductive Polymer Coating. *ACS Nano* **2011**, *5*, 9187−9193.
(49) Hart, C. J.; Cuisinier, M.; Liang, X.; Kundu, D.; Garsuch, A.; Nazar, L. F. Rational Design of Sulphur Host Materials for Li−S Batteries: Correlating Lithium Polysulphide Adsorptivity and Self−Discharge Capacity Loss. *Chem. Commun.* **2015**, *51*, 2308−2311.
(50) Li, W. Y.; Zheng, G. Y.; Yang, Y.; Seh, Z. W.; Liu, N.; Cui, Y. High−Performance Hollow Sulfur Nanostructured Battery Cathode Through a Scalable, Room Temperature, One−Step, Bottom−Up Approach. *Proc. Natl. Acad. Sci. U. S. A.* **2013**, *110*, 7148−7153.
(51) Li, H. F.; Yang, X. W.; Wang, X. M.; Liu, M. N.; Ye, F. M.; Wang, J.; Qiu, Y. C.; Li, W. F.; Zhang, Y. G. Dense Integration of Graphene and Sulfur via the Soft Approach for Compact Lithium/Sulfur Battery Cathode. *Nano Energy* **2015**, *12*, 468−475.
(52) Zu, C. X.; Fu, Y. Z.; Manthiram, A. Highly Reversible Li/Dissolved Polysulfide Batteries with Binder−Free Carbon Nanofiber Electrodes. *J. Mater. Chem. A* **2013**, *1*, 10362−10367.

DOI: 10.1021/acsami.5b04408
ACS Appl. Mater. Interfaces 2015, 7, 16715−16722